COBEM 2023 27TH INTERNATIONAL CONGRESS OF MECHANICAL ENGENEERING

ABCM Brazilian Society of Mechanical Sciences and Engineering
27th ABCM International Congress of Mechanical Engineering
December 04-08, 2023, Florianópolis-SC, Brazil

COB-2023-0493
ANALYSIS OF AERODYNAMIC DRAG IN A SQUAREBACK GEOMETRY BY NUMERICAL SIMULATION

Elisa Paola Mora Robles
epmorar@ufpso.edu.co
Mechanical Engineering - Francisco de Paula Santander University - Ocaña - IM/FI/UFPSO.
Vía Universidad Francisco de Paula Santander, Ocaña, NS, Colômbia
Internal Combustion Engines Laboratory - Joinville Technological Center - Federal University of Santa Catarina - LABMCI/CTJ/UFSC.
Rua Dona Francisca 8300, Joinville, SC, CEP 89219-600, Brazil.

Jorge Esteban Chavez Gutierrez
jorge.chavez@labmci.ufsc.br
Internal Combustion Engines Laboratory - Joinville Technological Center - Federal University of Santa Catarina - LABMCI/CTJ/UFSC.
Rua Dona Francisca 8300, Joinville, SC, CEP 89219-600, Brazil.

Carlos Javier Noriega Sanchez
cjnoriegas@ufpso.edu.co
Mechanical Engineering - Francisco de Paula Santander University - Ocaña - IM/FI/UFPSO.
Vía Universidad Francisco de Paula Santander, Ocaña, NS, Colombia

Leonel R Cancino
leonel.cancino@labmci.ufsc.br
Internal Combustion Engines Laboratory - Joinville Technological Center - Federal University of Santa Catarina - LABMCI/CTJ/UFSC.
Rua Dona Francisca 8300, Joinville, SC, CEP 89219-600, Brazil.

Abstract. *In vehicle design today, reducing fuel consumption is a top priority, which results in lowering pollution emissions, specifically the release of CO_2 into the environment. To achieve this goal, a variety of strategies have been identified, ranging from wind tunnel experiments to more recent utilization of computational fluid dynamics tools for numerical analysis. By utilizing simplified geometries, one can observe the primary attributes of the airflow pattern surrounding an actual vehicle. This includes the surface body's forces, such as side, drag, and lift, in addition to their respective moments. To achieve consistent numerical data, the ANSYS-FLUENT™ software tool was employed, and a numerical configuration was executed using data available in the literature. Mesh and computational domain independence tests were conducted to ensure data consistency. The fluid flow pattern was analyzed numerically, and resulting forces and momentum were estimated and compared to available literature. The results revealed that the turbulence model κ - ε realizable was the most accurate in determining the drag and lift coefficients compared to other models, with errors of 1.56% and 0.08%, respectively. Adding a spoiler to the rear of the geometry resulted in a 4.97% reduction in the drag coefficient and a 30.77% increase in the lift coefficient. The numerical simulation study conducted on a MIRA squareback geometry shows that installing a rear spoiler can improve fuel efficiency due to the drag force, which increases proportionately to the square of the velocity*

Keywords: *Vehicular aerodynamics, MIRA squareback geometry, Computational Fluid Dynamics, Turbulence Models*

1. INTRODUCTION

Vehicle usage has steadily increased worldwide, leading to higher fuel consumption and increased CO_2 emissions caused by engine operation. This phenomenon also correlates with vehicle aesthetics. Hence, the automotive industry is currently focused on designing new cars that provide optimal fuel efficiency to address these challenges. Additionally, a vehicle traveling at high speeds on the highway accounts for up to 50% of total fuel consumption. The vehicle experiences aerodynamic drag, wherein the drag force increases proportionally with the square of the speed. As a result, exceeding the speed limit generates higher fuel consumption (Çengel and Cimbala, 2017). Aerodynamics is the scientific study of airflow, specifically the effects and actions exerted by air on a moving vehicle, particularly its lower part. The two vital forces that comprise the aerodynamic force are called drag and lift (Fraija B., 2006). This field of study also encompasses ventilation, engine inlet and outlet flows, brake cooling, and the resulting forces acting upon the vehicle. The resistance to motion affects the shape and design of modern vehicles (Katz, 2016). Once the vehicle is in motion, it creates two

types of airflow- an external flow around the vehicle, resulting from the air passing over the surface, generating forces and moments, and an internal flow located in the engine, passenger compartment, exhaust system, and cooling system (Hucho, 1998).

Motor Industry Research Association (MIRA) are simplified car shapes that are one of the most popular reference geometries for wind tunnel and Computational Fluid Dynamics (CFD) studies. Although these models exhibit simplified geometry, they are remarkably similar to real vehicles in many respects. Salient characteristics of these shapes include smooth wheels without cavities, a smooth lower part, and an inclination angle of 10° in the engine hood, tilted side windows, and an upward-wrapping rear part. There are four MIRA reference geometries: Notchback, Squareback, Fastback, and Pick-Up (Musa and Patel, 2016). Thus, researchers use CFD in vehicle aerodynamics studies due to its high accuracy in supporting development. The use of CFD offers the benefits of low cost, time, and the ability to alter boundary conditions without any difficulty (Hu *et al.*, 2015).

In this sense, the objective of this research is to analyze the aerodynamics of this automotive reference geometry, especially the fluid field at the rear. The reference geometry is MIRA squareback, which has moderate aerodynamic drag, low rear lift and high rear sidewall. From a scale model, boundary conditions such as velocity at 25 m/s, air density and viscosity, atmospheric pressure, temperature and symmetry area are provided from the wind tunnel, information used as "input" to the CFD model / simulation for comparison with data found in the literature. For this purpose the turbulence models κ - ε realizable, κ - ε RNG, κ - ω and RSM, were then used. Among the main contributions of this work is the analysis of MIRA squareback geometry from the computational point of view, in order to elucidate the aerodynamic performance of this kind of geometry looking at drag and lift coefficients as the main representative data and comparing to experimental values reported in the literature. Additionally, was analyzed the aerodynamic perturbance caused by the modification of the base-model geometry when an up-rear spoiler is added.

2. METHODOLOGY

The MIRA squareback reference geometry was selected for investigating the aerodynamic forces in the squareback-like geometry vehicle. This geometry is a simplified version because of the lack of "real" vehicle details (doors, windows, mirrors, and has smooth wheels that do not rotate during the simulation). The geometry was used at a scale of 1:3 in the numerical simulations. Figure 1 shows the dimensions of the squareback geometry, with a cross-section area of 0.206 m^2.

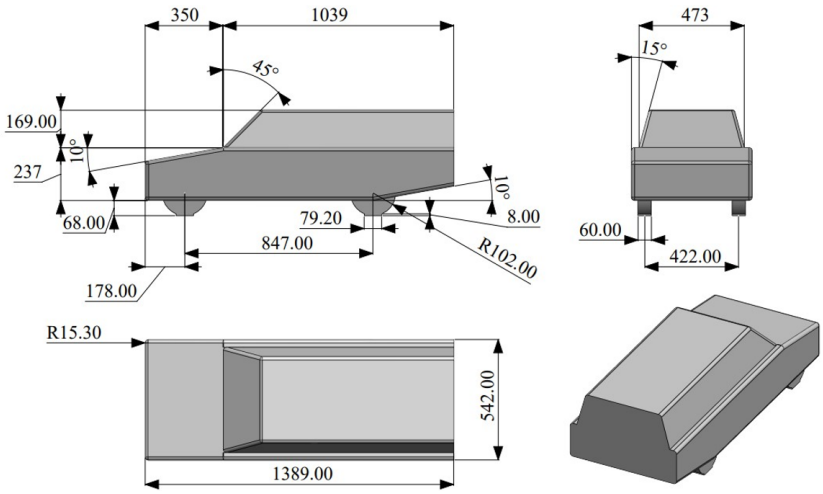

Figure 1. MIRA squareback reference geometry, dimensions in mm.

The computational domain is a decisive step in CFD analysis, as it influences the accuracy of the generated results (Sosnowski *et al.*, 2019). Sufficient space must be provided around the geometry so that the disturbances introduced by the geometry presence do not interfere with the boundaries themselves (Fröhlich *et al.*, 2005), in other words, the common wind tunnel measurements errors (Schutz, 2015; Hucho, 1998) must be avoided in the numerical simulation by using several strategies in boundary conditions as well as warranting space enough to attenuate the blockage effects (Carr and Stapleford, 1986; Choi and Lee, 2000)

2.1 Experimental data from literature

The experimental data for this investigation were taken from Wang *et al.* (2014), where tests were performed in the HD-2 boundary layer wind tunnel (Tongji University) with a cross-section of 3x2.5 m^2, with a closed horizontal circuit. The dimensions of the MIRA-squareback geometry were selected at a scale of 1:3 for wind tunnel testing. Table 1 presents the data used to calculate the Reynolds number, as well as input data utilized along the numerical simulations in

ANSYS-FLUENT™.

Table 1. Experimental from Wang *et al.* (2014) data used in this work

Velocity (m/s)	25	Reynolds (–)	1.4758 x 10^6	Density (kg/m^2)	1.2471	Length (m)	1.389
Wheelbase (m)	0.8470	Area (m^2)	0.103	Viscosity (m^2/s)	1.7894 x 10^{-5}	Temperature (°C)	288.16

The HD-2 wind tunnel reaches a maximum speed of 58 m/s. To eliminate the soil boundary layer, a boundary layer pumping system was installed ahead of the model under examination. The MIRA geometry's frontal area provides a blockage ratio lower than 5% and an average turbulence intensity below 0.2%. Pressure tapping along the symmetry plane was conducted using 46 pressure taps to assess the average pressure and calculate the pressure coefficient. The equipment utilized for the pertinent measurements consisted of an optic configuration situated atop the wind tunnel and a CCD camera chosen for experimentation. Velocity field measurements of the nearest wake were obtained using the 2D-1C system, without time resolution. The system, which was provided by Beijing Li Fang Tian Di (BLFTD) Technology Development Ltd., includes a double Nd Yag laser from Beamtech that emits laser pulses (532 nm, peak energy of 500 mJ/pulse) to illuminate the measurement position, forming a laser sheet. Approximately 200 double-frame images were obtained for the wake segments. The measurement position was placed in the plane of longitudinal symmetry where the near and far wake separated into four fields of view, each spaced 75 mm apart and located 1200 mm away from the rear. The quantitative and qualitative study from Wang *et al.* (2014) is a valuable starting point for developing aerodynamic studies on the MIRA geometry. Therefore, this study aimed to check the outcomes achieved from the numerical simulation conducted using ANSYS-FLUENT™.

2.2 Geometry, mesh parameters and mesh independence test

Two types of mesh were selected when creating the hybrid mesh: one formed by hexahedral elements around the surface of the squareback geometry, and the other by tetrahedral elements. To ensure quality, the geometry elements within the mesh undergo refinement, with an element size of 10 mm selected for each face of the geometry, except for the wheels, which have an element size of 2 mm. To adjust the elements and regulate the cell size, influence volumes are utilized to combine various types of elements within the mesh. Figure 2 illustrates the creation of the car-box influence geometry, positioned in the entire area of the geometry encompassing each surface of the squareback geometry. Next, the under-body box is constructed and placed between the ground surface and the wheels, which results in the removal of significant features around the wheels and rear area. To ensure accuracy in the simulation-generated data, a further influence volume has been created from the middle of the vehicle to the rear to obtain wake values. The creation of influence volumes for the geometry enables the mesh to attain appropriate velocity values, pressure, and boundary layer effects that are generated around the surface. Consequently, the mesh independence study defined the element size for each volume. The ANSYS-FLUENT™ software with the enclosure option was utilized to develop the computational domain. The main wind tunnel dimensions are shown in Figure 2, where a rectangular section was designed as reference for the relevant tests. Assuming flow symmetry, only half of the geometry was simulated since the forces are equal to those in the other half of the vehicle. According to literature, the distance from the velocity input to the front of the MIRA squareback geometry must be three times the length of the MIRA squareback (Fröhlich *et al.*, 2005).

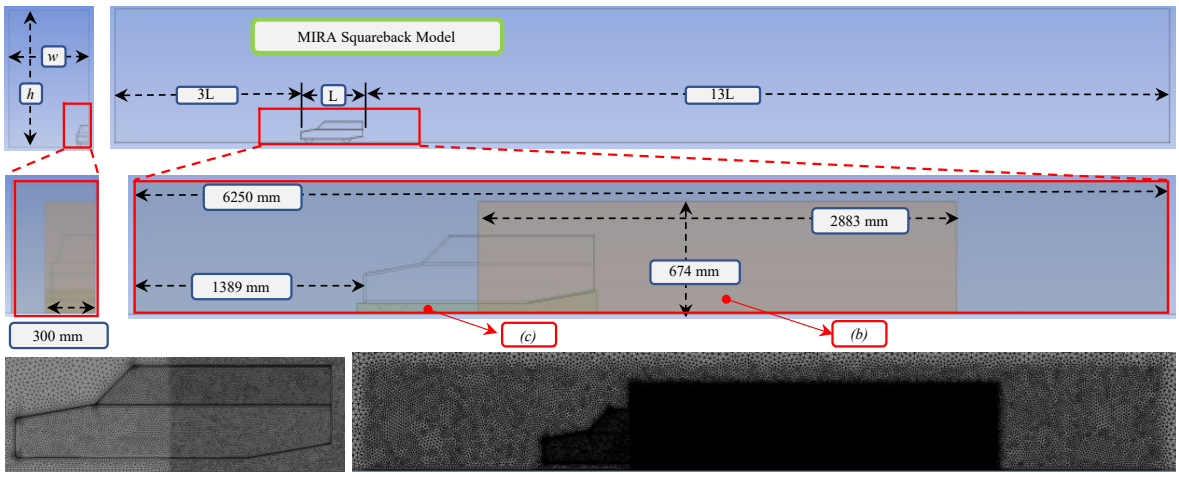

Figure 2. Dimensions of virtual wind tunnel and the boxes *(a)* Carbox, *(b)* Wakebox, *(c)* Underbox for mesh refinement purposes. The *w* and *h* correspond to the real wind tunnel used by Wang *et al.* (2014), and " L " represents the MIRA squareback length = 1389 mm.

The bottom of Figure 2 shows details of the the mesh refinements surrounding the entire MIRA squareback geometry. The figure shows the refinements made to each control volume and the two types of meshing, tetrahedral and hexahedral, to obtain the hybrid mesh.

2.3 Simulation set-up

The input data for each numerical simulation involves the values of velocity, density and Reynolds number from Table 1. Currently, computational fluid dynamics software has simplified the analysis of laminar flows; nevertheless, there is no one universal turbulence model for turbulent flow simulation. Therefore, developing a simulation with accurate fluid dynamic properties requires a specific turbulence model (Çengel and Cimbala, 2017). Four turbulence models were selected for simulation development, including κ - ε Realizable, κ - ε RNG, κ - ω Standard, and RSM. These models utilize two transport equations and different configurations to analyze flow behavior. The κ - ε Realizable model is particularly popular for aerodynamics simulations. Contains an alternate formulation for turbulent viscosity that satisfies mathematical constraints on Reynolds stresses consistent with the physics of turbulent flows (ANSYS-FLUENT, 2022). The κ - ε Realizable model has shown industry results with 2-5% accuracy (Lanfrit, 2005). The κ - ε RNG turbulence model adds a term to its equation that enhances accuracy for swift stress flows, eddy flows, and low Reynolds numbers. From another perspective, the κ - ω Standard turbulence model is an empirical model that utilizes the transport equations for turbulence, kinetic energy, and specific dissipation rate. It demonstrates high accuracy free shear flows. Finally, The Reynolds Stress Model (RSM) needs five extra 2D transport equations, while in 3D, it requires seven additional transport equations since it solves the transport equations to identify the Reynolds stresses and, together with another equation for the dissipation rate, closes the Reynolds Averaged Navier-Stokes equations (ANSYS-FLUENT, 2022). Figure 3 illustrates the wind tunnel boundary conditions used in this research for all simulation analyses. It depicts the interaction between the walls and the geometry, producing dependable results at the output.

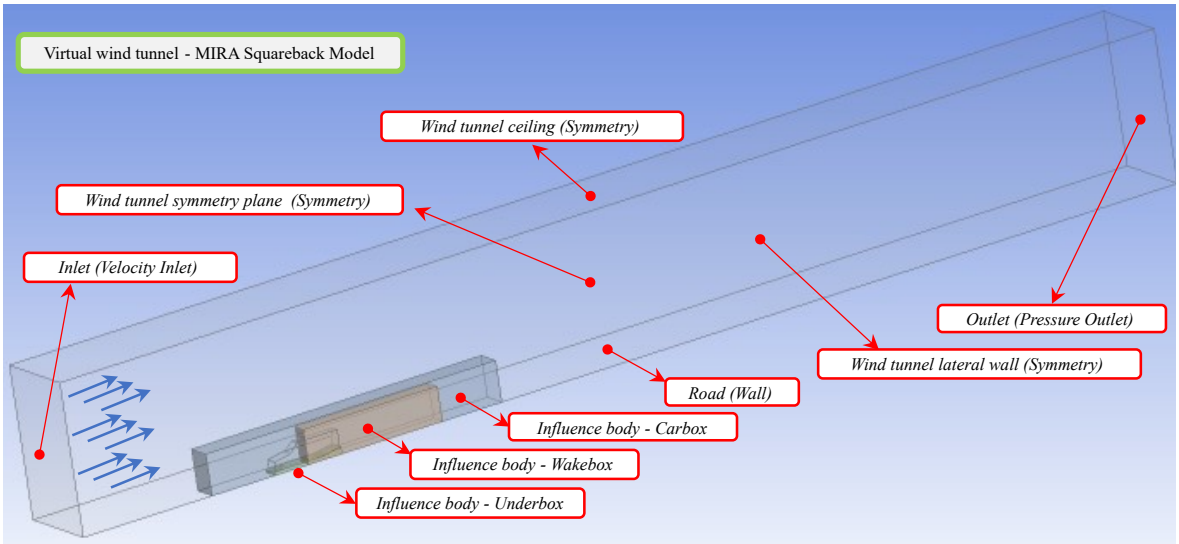

Figure 3. Boundary conditions used in this work for all the simulations

The simulations' development involves an inlet flow velocity of 25 m/s (90 km/h), following established boundary conditions. Turbulence intensity is determined by the mean square of turbulent velocity over mean flow velocity. ANSYS-Fluent recommendations specify turbulence range at 1% for velocity and 5% for pressure outlet boundary condition (ANSYS-FLUENT, 2022).

3. RESULTS AND DISCUSSION

For all the simulations, convergence was considered "acceptable" when the residuals of all the transport variables were below $1x10^{-4}$. In order to identify the virtual tunnel length and the minimum mesh size, independence test where then performed. The virtual tunnel cross section area is the same as in the experimental procedures of Wang *et al.* (2014), resulting in a blockage ratio of $\approx$2.751% which meets the requirement that the blockage ratio of the experimental model should be less than 5% (Choi and Lee, 2000). It should be noticed that numerically, the blockage criteria is also warranted.

3.1 Computational domain length and mesh size independence tests

The extension of the computational domain from the MIRA squareback rear to the wind tunnel exit, Figure 2 (for total length equal to 13L), was parametrized in function of the MIRA squareback geometry length (L), and then used for mesh independence analysis Figure 4. To investigate the response of the turbulence model, the length was changed from 5L to 15L during the simulation, where L refers to the total length of the squareback geometry (1389 mm). In the simulation, the sizes and refinement parameters of the car-box and under-body influence volumes remained constant for each study. However, for refinement, the weak-box influence volume underwent modification, proportional to the back length of the wind tunnel. This approach yielded a final length for conducting the mesh independence study. When the simulations began, the geometry was processed with a 51 mm edge rounding, determined from literature sources.

The drag coefficient (c_D) was utilized as assessment criteria along the mesh independence procedure and convergence criteria, using the κ - ε Realizable turbulence model. Figure 4(a) shows the mesh size independence test, which involved selecting a back length of 13L and varying the element size for the weak-box of 13, 10 and 8 mm, respectively. This allowed us to determine the c_D values and calculate the percentage difference between them. This information was used to determine the optimal mesh for the study with the other turbulence models. First, an appropriate element size is determined to ensure accurate results since meshes often yield varied outcomes. Thus, a mesh independence study with multiple refinements is selected to guarantee that the simulations results are not reliant on the number of elements in the mesh.

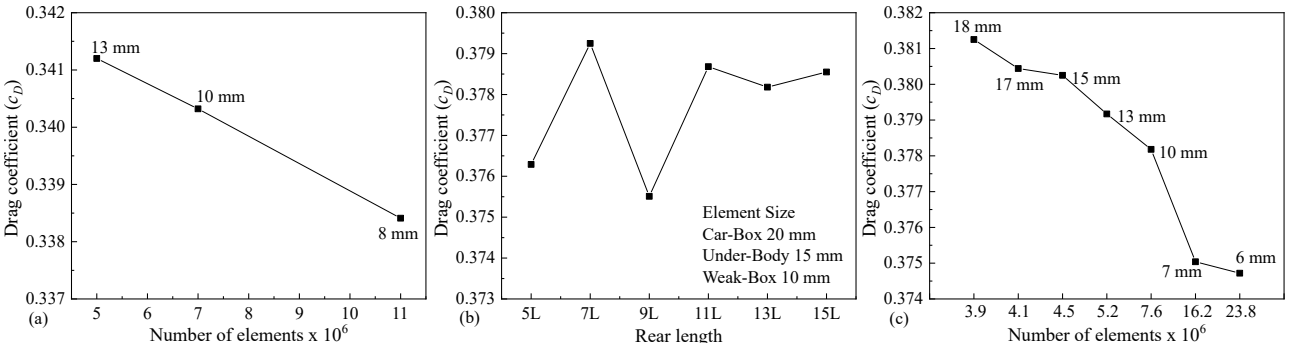

Figure 4. (a) Variation of the drag coefficient (CD) using a back length of 13L and element size for the weak-box of 13, 10 and 8 mm, respectively. (b) Mesh independence test for the rounding radius of 15.3 mm, computational domain length vs. Drag coefficient and, (c) Number of elements of mesh size vs. Drag coefficient with back length 13L (rounding radius of 15.3 mm).

Upon examining the c_D value obtained from the mesh independence test, specifically 0.3403, the error percentage is calculated using the experimental data reported by Wang *et al.* (2014) (c_D = 0.3842 and c_L = -0.3633), resulting in an error percentage of 11%. This percentage is notably high, and it is evident that the c_D obtained from the simulations consistently remained at a value of 0.34, without approaching the experimental value.

Therefore, changes were made to the geometry by reducing the edge radius. The radius was decreased by 50% and then by 70%, resulting in measurements of 25.5 mm and 13.5 mm, respectively, from the initial measurement of 51 mm. The 5L wind tunnel measurement was utilized for simulation, because of the proximity to the experimental value (Wang *et al.*, 2014). To determine the percentage error, a comparison of the drag and lift coefficients is necessary. This yields an approximate error of 2% for c_D and 0.7% for c_L, as shown in Table 2. To achieve these results, the edges were rounded to 13.5 mm and the simulation steps were taken as previously mentioned.

Table 2. Mesh study with edge radius reduction

Number of elements	Edge radius reduction	Rear length	c_D	% diff	c_L	% diff
5054446	50%	5L	0.3582	-6.7721	-0.3579	-1.4997
5075838	70%	5L	0.3766	-1.9808	-0.3607	-0.7031

The computational domain was set with a round radius of 13.5 mm, and the length of the wind tunnel varied between 5L and 17L. The car-box, under-body, and weak-box influence boxes had element sizes of 20mm, 15mm, and 10mm for the computational domain. The simulations were conducted with the intention of reaching convergence to determine the appropriate wind tunnel size for the mesh test. After setting the edge radius to 13.5 mm, 13L is selected as the length to proceed to the mesh test study. This resulted in an increase in drag coefficient compared to the initial values

obtained with a radius of 51 mm. Figure 4(b) illustrates that a convergence in drag coefficient occurs at 11L, which indicates the midpoint. The simulations were conducted using various refinements in the weak-box influence volume, as shown in Figure 4(c), and the results closest to the measured values were obtained. A length of 13L was chosen for the mesh independence test to determine the ideal mesh size, by using an element size of 10mm for wake-box (Figure 4(c)). The y^+ parameter determines the distance between the wall and the center of the element, and varies based on the selected turbulence model. The κ - ε model with non-equilibrium has a restriction of the y^+ to a range from $30 < y^+ < 300$ (ANSYS-FLUENT, 2014; MR-CFD, 2022). Figure 5(a) and (b) shows the y^+ and pressure coefficient fields on the square back geometry surface found in this work.

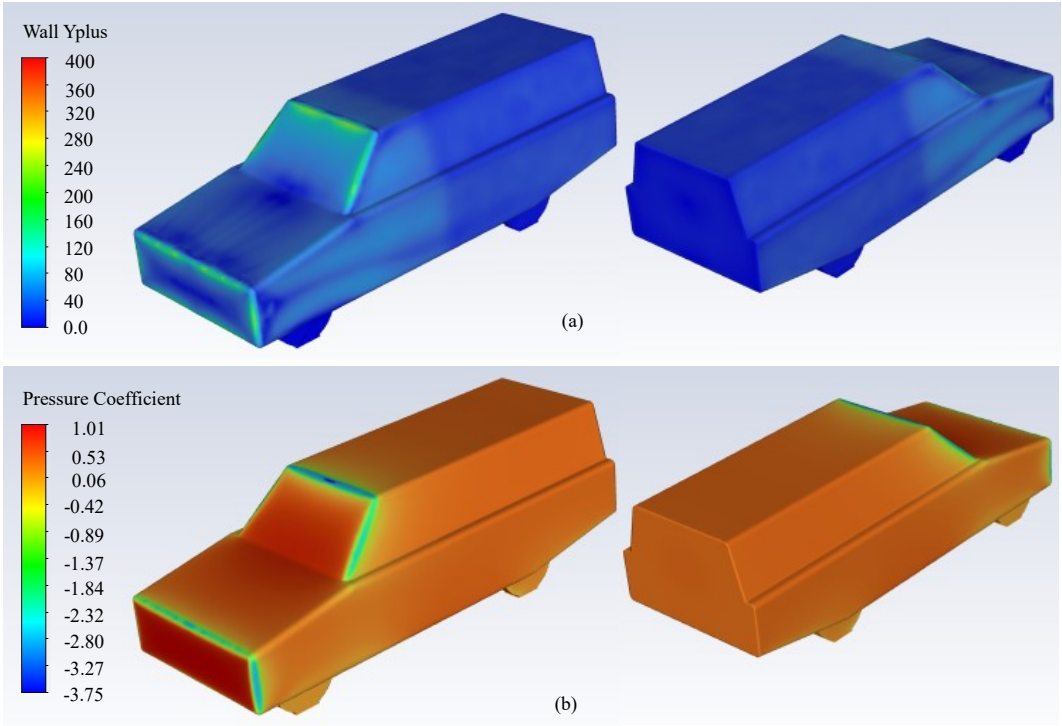

Figure 5. Fields of (a) y^+ and, (b) pressure coefficient found in the MIRA squareback geometry surface with turbulence model κ - ε Realizable.

3.2 Flow field

Experimental data reported in the literature (Hucho, 1998; Schutz, 2015) indicates that two vortex are commonly present in the rear-near wake region in squareback-type automotive geometries. The Figure 6 (a) and (b) from Wang *et al.* (2014) shows that couple of vortex at the same fluid conditions that those numerically analyzed in this work, with the upper vortex moving clockwise and the lower one moving counterclockwise. The Figure 6(c) shows the numerical response in terms of streamline field obtained in this work and compared to the numerical and experimental data from Wang *et al.* (2014). Should be notice that the main scale of both the vortex was adequately captured by the numerical simulation in this work.

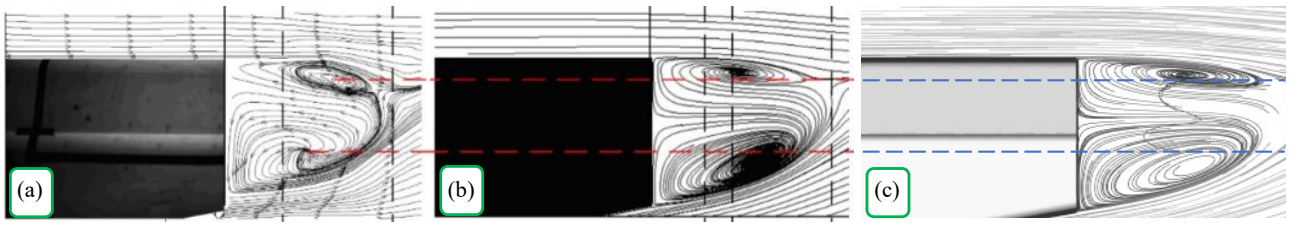

Figure 6. Streamline distribution along the longitudinal symmetry plane. (a) HD-2 wind tunnel experiments and (b) CFD simulation from Wang *et al.* (2014), (c) CFD simulation - this work

Furthermore, Figure 7 shows the velocity distribution in the symmetrical plane of the MIRA squareback geometry. At the vertical rear end of the geometry, a low-velocity area denoted (blue region) can be observed, which creates a pocket

responsible for the high-pressure area in this zone. The difference in pressure between the front and rear contributes significantly to aerodynamic drag. This, in real life, affects factors such as fuel efficiency, stability, and handling, among others. At the top right end part, the initial separation of the air fluid velocity can be observed. It has a high velocity compared to the velocity in the wake area. At the same time, this extreme airflow contributes to the development of the rotational vortex located at the top area of the wake. On the other hand, the airflow velocity near the rear wheel (bottom right) contributes to the development of the rotational vortex located at the bottom area of the wake.

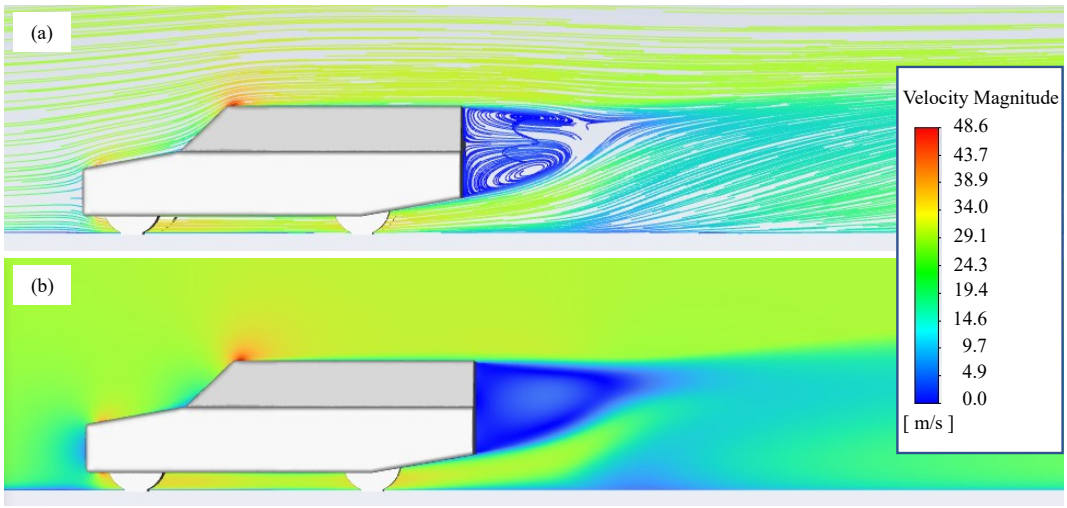

Figure 7. (a) Velocity pathlines at symmetry plane. (b) Velocity field at symmetry plane.

Figure 8(a) shows the pathlines by velocity magnitude. It can be observed the strong fluid interaction in the wake region. Along Figures 8(a) to (g), obtained at different but continuously z-plane (parallel to the squareback rear) , is possible to observe the interaction among the two vortex (Figure 6)(a) and the classical pair of vortex observed in the fastback and notchback automotive reference geometries Schutz (2015); Hucho (1998).

3.3 Drag and lift coefficients

Pressure and viscosity analysis (frictional drag) were carried out to measure the drag coefficient c_D using the κ - ε Realizable turbulence model in the MIRA squareback geometry. Face-naming allowed for the identification of high-pressure and high-friction areas. Negative values can be observed in Table 3, indicating that small low pressure areas are locally present, acting in the negative direction of the main flow stream.

Then, the analysis of the drag and lift coefficients was carried out with each named zone, using the four turbulence models i.e. κ - ε Realizable, κ - ε RNG, κ - ω Standard and RSM, where it could be observed that in each model in the front and upper front zones the c_D was negative, showing that in these areas there is flow separation, see Table 3. It was also observed that the κ - ω Standard model had a higher c_D than the other models and that the κ - ε RNG model had a higher c_L.

Table 3. Drag and lift coefficients contributions of each named zone (surface) of MIRA squareback geometry

Zone name	**κ - ε Realizable**		**κ - ε RNG**		**κ - ω Standard**		**RSM**	
	c_D	c_L	c_D	c_L	c_D	c_L	c_D	c_L
Floor	0.06608	-0.98647	0.06152	-0.9489	0.06268	-0.93429	0.062	-0.95832
Front	-0.00235	0.02358	-0.01232	0.06779	-0.00512	0.03703	-0.00533	0.03875
Front Wheels	0.03982	0.00163	0.04057	0.00435	0.04158	0.004	0.04047	0.00283
Lower side	0.00947	0.02934	0.00688	0.03063	0.00893	0.02939	0.00984	0.02963
Lower top	0.14803	0.00862	0.16814	0.00312	0.16084	0.01084	0.15031	0.00803
Rear	0.1173	-0.00006	0.10738	-0.00005	0.11198	-0.00013	0.12058	-0.00004
Rear Wheels	0.03086	-0.01567	0.03774	-0.00689	0.03506	-0.01138	0.02745	-0.01306
Side	0.00502	0.12004	0.00544	0.11541	0.00527	0.1192	0.00581	0.11558
Top	0.00488	0.35705	0.0039	0.36533	0.00508	0.35091	0.00512	0.35857
Top Front	-0.0409	0.09574	-0.02913	0.08315	-0.03396	0.08607	-0.04389	0.10083
Total	0.37819	-0.36621	0.39013	-0.28607	0.39234	-0.30835	0.37235	-0.31720

Similarly, the simulation results of each turbulence model for the aerodynamic coefficients were then compared to the literature's experimental values as presented in Table 4. In terms of error percentages, the κ - ε Realizable model shows to be the better method for determining drag and lift coefficients, while the κ - ε RNG, κ - ω Standard, and RSM models

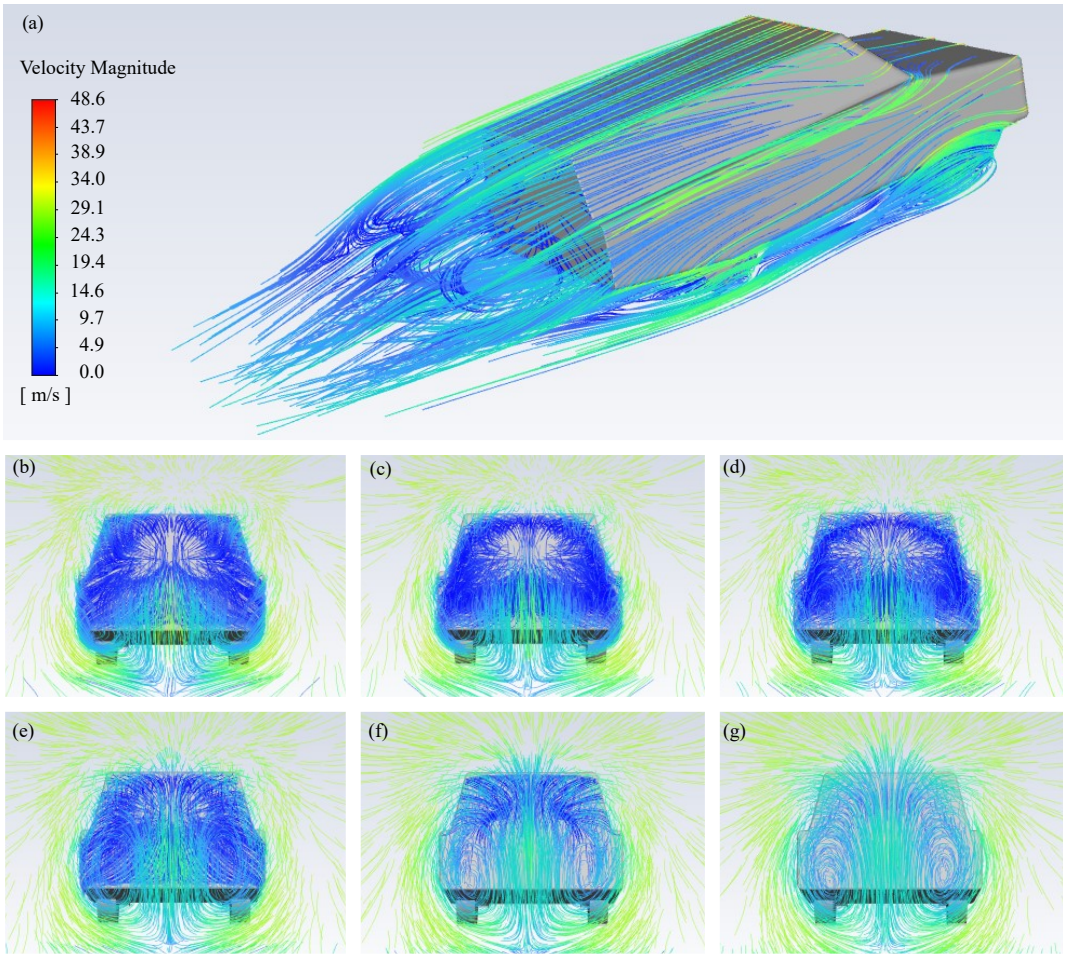

Figure 8. Velocity pathlines at several z-plane locations (from the rear) in the wake. (a) 3D-view, (b) z = 5 cm, (c) z = 15 cm, (d) z = 25 cm, (e) z = 35 cm, (f) z = 45 cm, (g) z = 55 cm,

are suitable for calculating drag coefficients with acceptable error. However, when it comes to lift coefficients, there is an increase in error percentage due to the equations each model employs, rendering them adequate for only one aerodynamic coefficient.

Table 4. Percentage error of aerodynamic coefficients for each turbulence model

Turbulence model	c_D Exp (0.3842) % diff	c_L Exp (-0.3633) % diff	Turbulence model	c_D Exp (0.3842) % diff	c_L Exp (-0.3633) % diff
κ - ε Realizable	-1.56%	0.08%	κ - ω Standard	2.12%	-15.12%
κ - ε RNG	-1.54%	-21.26%	RMS	-3.08%	-12.69%

3.4 Modification of the MIRA squareback geometry

In this section, the geometry was modified by incorporating a spoiler on the rear upper portion as shown in Figure 9(a). The objective was to decrease the drag coefficient, which required an enhancement in the pressure at the back. Computational domain studies and mesh independence tests were conducted to ascertain the reduction of the drag coefficient using the κ - ε Realizable turbulence model. The measurements and element size of the influence volumes, car-box of 20 mm and under-body of 15 mm for the geometry analysis without spoilers, were initially retained. The simulations were run until they converged, selecting the wind tunnel size for the mesh test. When determining the 13L length, a mesh independence test was performed. The test involves adjusting the size of the weak-box element and is illustrated in Figures 9(b) and (c).

The c_D decreased following the spoiler's addition, while the c_L increased. For comparison, the previous simulation results are used as a reference since the same turbulence model and boundary conditions were applied (see Table 5).

The modifications in the wake are also noticeable in the rear section of the geometry, as depicted in Figure 10 when

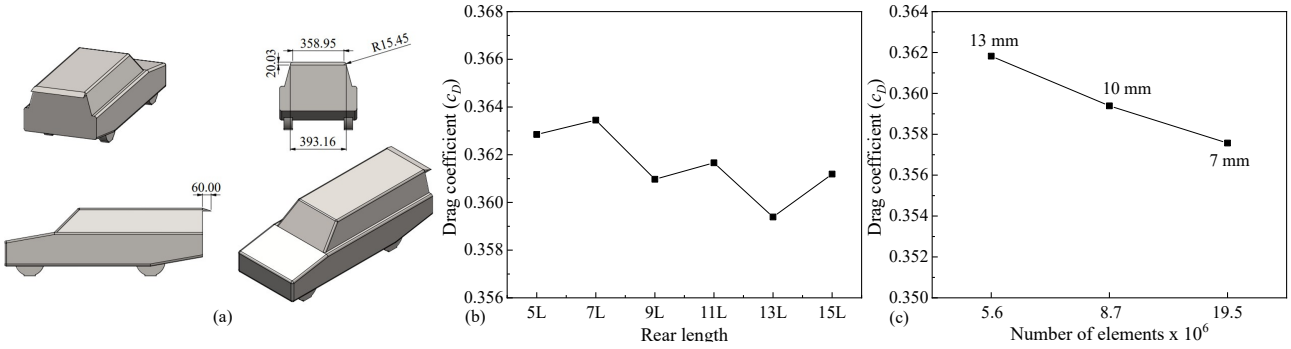

Figure 9. (a) MIRA squareback geometry with addition of spoiler – Dimensions in mm. (b) Computational domain length independence test with the addition of spoiler. (c) Mesh size independence test with the addition of spoiler.

Table 5. Comparison of the aerodynamic coefficients of squareback geometry with and without spoilers

Aerodynamic Coefficient	MIRA squareback (base model)	MIRA squareback with spoiler	% diff
c_D	0.37819	0.35939	-4.97%
c_L	-0.36621	-0.25352	-30.77%

comparing to Figure 7. Here, the vortex core moved closer to the rear, modifying the fluid flow pattern in relation to the base model, resulting in a decrease in the drag coefficient.

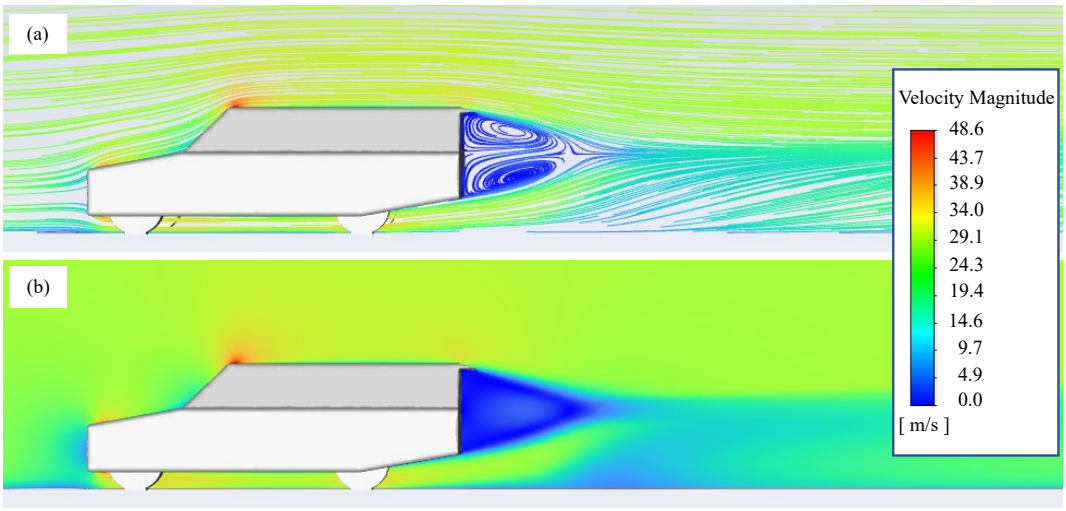

Figure 10. Modified squareback geometry. (a) Velocity pathlines at symmetry plane. (b) Velocity field at symmetry plane.

4. CONCLUSIONS

In the present work, a MIRA squareback geometry was analyzed numerically using ANSYS-FLUENT™ software and a hybrid meshing strategy. The main conclusions of this work can be summarized as follows:

- The κ - ε Realizable turbulence model was used, and the study aimed to analyze the convergence of the drag coefficient (c_D) by carrying out computational domain simulations to determine the back length of the wind tunnel. This allowed for the development of the wake and separation of the boundary layer without interference. Numerical results compared to the experimental ones assess the performance of turbulence model.

- The mesh independence test allows the appropriate elements numbers for conducting the study with the mesh being independent of size. The c_D results were validated using literature data. Initially, with an edge rounding radius of 51 mm, a percentage error of 11% was obtained compared to the literature. Subsequently, sequential simulations were able to obtain percentage values of 1.56% for the c_D and, simultaneously, 0.08% for the lift coefficient using an edge rounding radius of 13.5 mm.

- It was observed that the κ - ε Realizable model exhibits the lowest percentage of error in terms of aerodynamic coefficients in comparison to other models, including the κ - ε RNG model. Although the κ - ε RNG model improves its equation to increase accuracy, it is not as close to the literature values. The κ - ω Standard model, and the RMS turbulence model yield high lift coefficient results but acceptable values for the drag coefficient.

- Finally, adding a spoiler to the upper rear section of the MIRA squareback design reduces the drag coefficient by altering the wake structure. Compared to the spoiler-less geometry, the vortex cores are closer to the rear area, modifying the flow field and of this form reducing the drag coefficient. The reduction of the drag coefficient results in an increase in the lift coefficient, which improves stability at higher speeds and in crosswinds. The numerical simulation study of the MIRA squareback geometry, with the addition of a spoiler, also suggests that fuel consumption can be improved due to the reduction in drag coefficient

5. ACKNOWLEDGEMENTS

The authors would like to acknowledge the support of UFSC Joinville TI team (Mr. Kleber Carlos Francisco) for all support given to the LABMCI computer network. The financial help for the undergraduate exchange of Ms. Elisa Paola Mora Robles at LABMCI/CTJ/UFSC from the *Oficina de Relaciones Internacionales - ORI* at the Francisco de Paula Santander University, Ocaña Campus - is also appreciated.

6. REFERENCES

ANSYS-FLUENT, 2014. "Ansys fluent lecture 7: Turbulence modeling - introduction to ansys fluent 15.0 release". ANSYS Confidential.

ANSYS-FLUENT, 2022. "ANSYS Fluent Technical Documentation - 2022R2".

Carr, G.W. and Stapleford, W.R., 1986. "Blockage Effects in Automotive Wind-Tunnel Testing". p. 860093. doi: 10.4271/860093. URL `https://www.sae.org/content/860093/`.

Çengel, Y. and Cimbala, J., 2017. *Fluid Mechanics: Fundamentals and Applications*. McGraw Hill, New York, NY, 4th edition. ISBN 978-1-259-69653-4.

Choi, J.H. and Lee, S.J., 2000. "GROUND EFFECT OF FLOW AROUND AN ELLIPTIC CYLINDER IN A TURBULENT BOUNDARY LAYER". *Journal of Fluids and Structures*, Vol. 14, No. 5, pp. 697–709. ISSN 0889-9746. doi:10.1006/jfls.2000.0290.

Fraija B., I., 2006. "Estudio de la aerodinámica en los vehículos". *PROSPECTIVA*, Vol. 4, pp. 66 – 70. ISSN 1692-8261. URL `https://www.redalyc.org/articulo.oa?id=496251108011`.

Fröhlich, J., Mellen, C.P., Rodi, W., Temmerman, L. and Leschziner, M.A., 2005. "Highly resolved large-eddy simulation of separated flow in a channel with streamwise periodic constrictions". *Journal of Fluid Mechanics*, Vol. 526, pp. 19–66. ISSN 1469-7645, 0022-1120. doi:10.1017/S0022112004002812. Publisher: Cambridge University Press.

Hu, X.J., Yang, H.B., Yang, B., Li, X.C. and Lei, Y.L., 2015. "Effect of Car Rear Shape on Pollution Dispersion in Near Wake Region". *Mathematical Problems in Engineering*, Vol. 2015, p. e879735. ISSN 1024-123X. doi: 10.1155/2015/879735. Publisher: Hindawi.

Hucho, W.H., ed., 1998. *Aerodynamics of Road Vehicles: From Fluid Mechanics to Vehicle Engineering*. SAE INTL, Warrendale, PA, 4th edition. ISBN 978-0-7680-0029-0.

Katz, J., 2016. *Automotive Aerodynamics*. Wiley, Chichester, West Sussex, 1st edition. ISBN 978-1-119-18572-7.

Lanfrit, M., 2005. "Best practice guidelines for handling Automotive External Aerodynamics with FLUENT".

MR-CFD, 2022. "Y-plus application in cfd simulation". `https://www.mr-cfd.com/y-plus-application-in-cfd-simulation/`. Accessed: 2022-08-01.

Musa, J.K. and Patel, P., 2016. "Aerodynamic Drag Reduction of a Passenger Vehicle by Controlling the Wake Using CFD Analysis". *International Journal For Science Technology And Engineering*, Vol. 2, No. 11, pp. 282–288. URL `https://ijste.org/Article.php?manuscript=IJSTEV2I11178`.

Schutz, T., ed., 2015. *Aerodynamics of Road Vehicles*. SAE International, Warrendale, Pennsylvania, 5th edition. ISBN 978-0-7680-7977-7.

Sosnowski, M., Gnatowska, R., Grabowska, K., Krzywański, J. and Jamrozik, A., 2019. "Numerical Analysis of Flow in Building Arrangement: Computational Domain Discretization". *Applied Sciences*, Vol. 9, No. 5, p. 941. ISSN 2076-3417. doi:10.3390/app9050941. Publisher: Multidisciplinary Digital Publishing Institute.

Wang, Y., Xin, Y., Gu, Z., Wang, S., Deng, Y. and Yang, X., 2014. "Numerical and Experimental Investigations on the Aerodynamic Characteristic of Three Typical Passenger Vehicles". *Journal of Applied Fluid Mechanics*, Vol. 7, No. 4, pp. 659–671. ISSN 1735-3572. doi:10.36884/jafm.7.04.21460.

7. RESPONSIBILITY NOTICE

The authors are solely responsible for the printed material included in this paper.